Received: 9 October 2021 | Revised: 14 July 2022 | Accepted: 18 July 2022

DOI: 10.1002/joc.7811

RESEARCH ARTICLE

International Journal of Climatology RMetS

Climate change projection over Mainland Southeast Asia and the Lancang-Mekong River basin based on a set of RegCM4 simulations

Yuanhai Fu[1] | Xuejie Gao[1,2,3] | Ying Xu[4] | Filippo Giorgi[5]

[1]Climate Change Research Center, Institute of Atmospheric Physics, Chinese Academy of Sciences, Beijing, China

[2]Collaborative Innovation Center on Forecast and Evaluation of Meteorological Disasters, Nanjing University of Information Science & Technology, Nanjing, China

[3]University of Chinese Academy of Sciences, Beijing, China

[4]National Climate Center, China Meteorological Administration, Beijing, China

[5]The Abdus Salam International Centre for Theoretical Physics, Trieste, Italy

Correspondence

Xuejie Gao, Climate Change Research Center, Institute of Atmospheric Physics, Chinese Academy of Sciences, Beijing, China.
Email: gaoxuejie@mail.iap.ac.cn

Funding information

Strategic Priority Research Program of the Chinese Academy of Sciences, Grant/Award Number: XDA2006040102; National Natural Science Foundation of China, Grant/Award Number: 41675103; Science and Technology Program of Yunnan, Grant/Award Number: 2018BC007

Abstract

We investigate the projected climate change over Mainland Southeast Asia (also known as the Indochina Peninsula) and the Lancang-Mekong River basin, a region with complex topography and unique weather and climate systems, but limited availability of published high-resolution regional climate model (RCM) studies. The study is based on an unprecedented ensemble of 21st century projections with the RegCM4 RCM driven by five different general circulation models (GCMs) at a grid spacing of 25 km under the representative concentration pathways RCP4.5 and RCP8.5. We focus on mean temperature and precipitation in the dry season November–March (NDJFM), the wet season May–September (MJJAS), and the whole year. Intercomparison between the RegCM4 simulations with the driving GCMs is provided to illustrate the added value of the RegCM4 experiments. RegCM4 reproduces greater and more realistic spatial detail of the present day temperature and precipitation distribution compared to the driving GCMs, but some biases are found, such as an overestimation of precipitation over high topography regions. The spatial pattern of biases shows some consistencies across the GCMs and, for NDJFM the RegCM4, although weak correlation is found between the GCM and nested RegCM4 biases. A generally lower warming is projected in the future by the RegCM4 in different seasons and the whole year. For precipitation, while prevailing increases are found in the GCM projections, large areas of decrease occur in the RegCM ones, in particular during the wet season, possibly due to the more detailed topographical representation. The change patterns of precipitation show consistencies across the GCMs and the RegCM4, especially in MJJAS. The projected changes of extreme indices indicate a general decrease/increase of extreme cold/warm events. Drought events are projected to be more frequent over the southwestern, while a general increase of heavy rain events prevails over most parts of the region.

KEYWORDS

climate change, Lancang-Mekong River basin, Mainland Southeast Asia, regional climate model

1 | INTRODUCTION

Mainland Southeast Asia (MSEA, also known as the Indochina Peninsula) is the continental part of Southeast Asia and it includes Vietnam, Laos, Cambodia, Myanmar, Thailand, Malaysia (Peninsular part), and Singapore. Dominated by monsoon climate, the region suffers frequently from flood and drought disasters and is considered as one of the most vulnerable regions to climate change due to its high exposure and low resilience (Hijioka *et al.*, 2014).

The Lancang-Mekong River (LMR) is the largest river in MSEA, with an estimated length of 4,880 km and a drainage area of 795,000 km^2 (MRC, 2005; 2010). It flows from the Tibetan Plateau to the South China Sea through six countries: China, Myanmar, Thailand, Laos, Cambodia, and Vietnam. The basin (LMRB) area is shared among China (21%), Myanmar (3%), Laos (25%), Thailand (23%), Cambodia (20%), and Vietnam 59 (8%). It provides food, water, transport, and other resources for daily life to the over 70 million people living in the region.

The MSEA has experienced significant changes in climate during late decades, including an increase of average surface temperature, frequency of heat waves, and occurrence of heavy precipitation events (Manton *et al.*, 2001; Tangang *et al.*, 2007; Hijioka *et al.*, 2014; Fan and He, 2015; Overland *et al.*, 2017; Supari *et al.*, 2017; Thirumalai *et al.*, 2017; Ge *et al.*, 2019a; Irannezhad *et al.*, 2020). For example, Thirumalai *et al.* (2017) reported that global warming increases the likelihood of record-breaking temperature extreme events over the region. Ge *et al.* (2019a) found that MSEA has been undergoing a significant warming trend of $0.37^{\circ}C\cdot decade^{-1}$ over the past 30 years. Irannezhad *et al.* (2020) showed substantial increases/decreases in precipitation over the northern/western parts of the Mekong River Basin during 1952–2015, which caused significant wetting/drying trends.

Therefore, understanding the characteristics of future climate change over the MSEA and LMRB is crucial in order for the region to implement proper adaptation and mitigation measures. Thus how the climate over the MSEA and LMRB will change in the future?

As primary tools for projecting future climate change, general circulation models (GCMs) of different generations have been applied over the region (Christensen *et al.*, 2007; Huang *et al.*, 2014; Ruan *et al.*, 2019; Chhin *et al.*, 2020; Iqbal *et al.*, 2021; Liu *et al.*, 2021; Supharatid *et al.*, 2022). For example, Huang *et al.* (2014) evaluated the performance of GCMs participating in the Coupled Model Intercomparison Project Phase 5 (CMIP5; Taylor *et al.*, 2012) in simulating temperature over LMRB and provided futures changes by Bayesian multimodel averaging methods. Ruan *et al.* (2019) applied an improved score-based method to analyse the output in CMIP5 GCMs and found a large discrepancy in the magnitudes of changes in future temperature over the MSEA region. More recently, Iqbal *et al.* (2021) evaluated the performance of CMIP6 modes in simulating precipitation over the MSEA and found that only less than one-tenth of models are able to reproduce the observed precipitation climatology. Finally, Supharatid *et al.* (2022) also found that the CMIP6 models show large intermodel discrepancies in reproducing the observed temperature and precipitation characteristics over the MSEA.

In general, deficiencies of GCMs due to their coarse spatial resolutions (typically ranging from 100 to 200 km) limit their skill in simulating regional and subregional climate change, in particular over the MSEA and LMRB, which are characterized by complex topography and unique weather and climate system. Thus, regional climate models (RCMs) can be especially used to downscale the GCM simulations (Giorgi and Gao, 2018; Giorgi, 2019) and obtain finer scale information over the region.

Several studies have been conducted on projecting future changes in mean and extreme climate variables over Southeast Asia by RCMs, either for the whole region or different parts/countries, most notably based on the Southeast Asia Regional Climate Downscaling/Coordinated Regional Climate Downscaling Experiment–Southeast Asia (SEACLID/CORDEX-SEA) (Giorgi *et al.*, 2009; Katzfey *et al.*, 2016; Ngo-Duc *et al.*, 2017; Tangang *et al.*, 2018; Ge *et al.*, 2019b; Nguyen-Thuy *et al.*, 2020; Sun *et al.*, 2020; Supari *et al.*, 2020; Tangang *et al.*, 2020; Nguyen-Ngoc-Bich *et al.*, 2021). Among these studies, Katzfey *et al.* (2016) presented an evaluation of the ability of two high-resolution RCMs in simulating temperature and precipitation over Vietnam during 1980–2000. Nguyen-Thuy *et al.* (2020) and Nguyen-Ngoc-Bich *et al.* (2021) projected future changes of climate in Vietnam using the output of the SEACLID/CORDEX-SEA simulation ensemble, while Tangang *et al.* (2018, 2020) and Supari *et al.* (2020) investigated future climate change over the whole Southeast Asia region in the same ensemble.

Although the SEACLID/CORDEX-SEA initiative provides a good base dataset to investigate climate change issues over Southeast Asia, studies focusing on the MSEA and LMRB are still very limited, and can be complemented by additional simulations including this region in their domain, such as the CORDEX East Asia one (e.g., Gao *et al.*, 2018). In this regard, a set of 21st-century projections was completed using the Abdus Salam International Center for Theoretical Physics Regional Climate Model version 4 (RegCM4; Giorgi *et al.*, 2012) driven by different GCMs over the CORDEX Phase II East Asia region (available at https://cordex.org/domains/region-7-east-asia/) (Gao *et al.*, 2018). This is one of the largest ensembles available with a RCM for the East Asia domain and while the design of the model domain is focused more on East Asia, most of the MSEA is included except for Peninsular Malaysia in the southern part of the Malay Peninsula. Similarly, analyses of these simulations so far have mostly focused on mainland China (e.g., Gao *et al.*, 2018; Gao and Zhang, 2020; Tong *et al.*, 2020; Wu and Gao, 2020), or tropical cyclones over the western North Pacific (Wu *et al.*, 2021). Therefore, this dataset offers new opportunities to investigate climate change projections for the Indochina peninsula.

In particular, in the present study, we complement and extend previous work in that: (a) we focus not only on mean changes but also on a range of indicators of extreme temperature and precipitation events of relevance for impact applications; (b) we intercompare RCM and driving GCM results in order to quantify the added value of the downscaling runs over the regions; (c) we assess the importance of the more detailed RCM representation of local forcings, such as topography and land use. In addition, our ensemble employs a different domain compared to that used in CORDEX-SEA.

A brief introduction of the simulations is provided in the next section, while validation of the model performances and projected changes are discussed in sections 3 and 4, respectively. Finally, conclusion and discussion are provided in section 5.

2 | MODEL AND DATA

Five GCMs from the CMIP5 program are used to drive the RegCM4 projections: CSIRO-Mk3-6-0, EC-EARTH, HadGEM2-ES, MPI-ESM-MR, and NorESM1-M (Rotstayn *et al.*, 2010; Hazeleger *et al.*, 2010; Collins *et al.*, 2011; Bentsen *et al.*, 2013; Iversen *et al.*, 2013; Jungclaus *et al.*, 2013; Stevens *et al.*, 2013, respectively). These five GCMs were selected due to their relatively high-resolution within the CMIP5 ensemble, the data availability, and their relatively good performance over the East Asia region (Jiang *et al.*, 2016). The five GCMs are hereafter referred to as CSIRO, EC, Had, MPI, and Nor, with the corresponding RegCM4 simulations as CdR, EdR, HdR, MdR, and NdR, respectively.

The GCMs provide initial and 6-hourly driving lateral boundary conditions for wind components, temperature, surface pressure and water vapour mixing ratio, along with time varying sea surface temperature (SST). The RegCM4 is run at a grid spacing of 25 km with 18 vertical sigma levels and model top at 10 hPa. The configuration of the model follows Gao *et al.* (2016, 2017), with land cover data updated over China as in Han *et al.* (2015) to represent more realistic vegetation cover compared to the standard RegCM4 configuration. Figure 1a,b shows the region of interest (MSEA, 90°–110°E, 8°–35°N), and topography for the GCM average and the RegCM4, respectively. The better description of the topography and coast lines in RegCM4 is evident compared to the

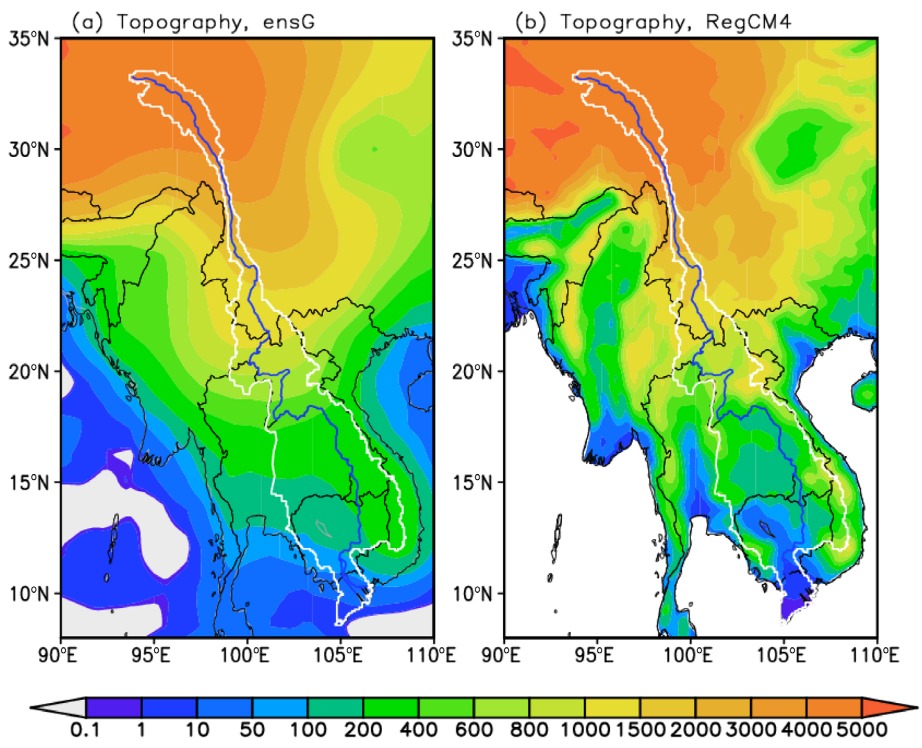

FIGURE 1 Region of interest and topography of (a) the GCMs and (b) RegCM4 (the blue line indicates the Lancang-Mekong River, and the white line indicates the Lancang-Mekong River basin). Unit: m

driving GCMs. Most notably, the land extends far into the bay and gulfs in the GCMs due to their coarse resolution.

The RegCM4 simulations cover the historical period 1971–2005 using observed greenhouse gas (GHG) concentrations, and the 2006–2098 future period under the RCP4.5 and RCP8.5 concentration scenarios (Gao *et al.*, 2018). We focus our analysis on RCP4.5, which lies towards the mid of the full CMIP5 scenario range, with regional mean changes under high-end RCP8.5 are also provided. Here 1995–2014 is used as present day reference period, 2041–2060 as mid-21st century and 2079–2098 as end of 21st century, as adopted in the Intergovernmental Panel on Climate Change Sixth Assessment Report (IPCC AR6; Lee *et al.*, 2021).

Observations of daily mean temperature and precipitation employed to validate the simulations are taken from the gridded observational dataset CN05.1 (Wu and Gao, 2013) inside the Chinese territory, and the Asian Precipitation Highly Resolved Observed Data Integration Towards Evaluation (APHRODITE) in the remaining regions (Yatagai *et al.*, 2012). For daily mean, maximum, and minimum temperature, we use the Climate Prediction Center (CPC) Global Daily Temperature (https://psl.noaa.gov/data/gridded/data.cpc.globaltemp.html) dataset outside China and CN05.1 within the Chinese territory. The RegCM4 and GCM outputs and the CPC dataset are bilinearly interpolated to the CN05.1 and APHRODITE common grid at 0.25° × 0.25° (latitude × longitude) resolution.

We focus on the ensemble mean temperature and precipitation in the dry season of November–December–January–February–March (NDJFM, also the cold season), the wet season of May–June–July–August–September (MJJAS, the warm season), and the whole year. Model validation and intercomparison for both the present day simulation and future projections between the RegCM4 and driving GCMs are provided. In addition, two indices for temperature, TNn and TXx (the annual minimum and maximum of daily minimum and maximum surface temperature) and two for precipitation, CDD (maximum annual number of consecutive dry days) and Rx5day (the annual maximum consecutive 5-day precipitation) are used to assess the projected changes in extremes by RegCM4.

3 | VALIDATION OF THE PRESENT DAY CLIMATE PERIOD

3.1 | Temperature

Figure 2 presents the mean temperature from the ensemble of the five GCM (ensG) and five RegCM4 simulations (ensR) along with observations in the dry and wet seasons, and the whole year. In the observations (Figure 2a–c), tropical climate dominates the southern part of the region, with temperatures higher than 25.0°C prevailing throughout the year. In the northern part, both a latitudinal and a topographic dependence is found, with the lowest temperatures (lower than −10.0°C) occurring during the dry season over the southeastern part of the Tibetan Plateau. Regional mean temperatures over the LMRB in the dry season, wet season, and whole year are 19.9, 24.2, and 22.3°C, respectively.

The broad pattern of the observed temperature is reproduced by both ensG and ensR; however, ensR clearly provides enhanced spatial detail in closer agreement with observations (Figure 2g–i). The steep topographic temperature gradient, as well as the higher temperatures in the Irrawaddy and Chao Phraya valleys compared to the watersheds, are realistically reproduced in ensR but not in ensG. A general cold bias prevails in both ensG and ensR in all seasons and the annual mean (figure not shown for brevity), with the bias being greater in the dry than the wet season. The regional mean biases over the LMRB in the dry season, wet season, and whole year are −2.9, −1.0, and −1.8°C for ensG, and −2.7, −1.3, and −1.9°C in ensR, respectively, indicating the strong contribution of the GCM forcings in determining the region-averaged ensemble biases.

The agreement between simulated and observed temperatures over MSEA region for each simulation is further evaluated using Taylor diagrams (Taylor, 2001) (Figure 3a), which provides a measure of performance in reproducing the spatial patterns of a variable. The GCMs reproduce the temperature patterns better in the dry season and the whole year, compared to the wet season. The improvements obtained using the RegCM4 are significant, and with a lower spread compared to the GCMs, due to the strong contribution of local topographic features. In the RegCM4 runs, the values for the spatial correlation coefficients are close to or larger than 0.90, the normalized standard deviation ranges from 1.0 to 1.5, and the centred root-mean-square errors around 0.50, clearly illustrating the added value of the downscaling runs.

Following Gao *et al.* (2012) and Wu and Gao (2020), we calculated the spatial correlation coefficients (CORs) of the temperature biases across the model simulations over the MSEA (Table 1), to assess the intermodel variability and how it is transferred from the GCM to the RegCM4 runs. As shown in the table, good correlations are found across the GCM simulations in both NDJFM and MJJAS biases. The CORs across RegCM4 simulations are also large, mostly greater than 0.90; however, the correlations between the RegCM4 simulations and

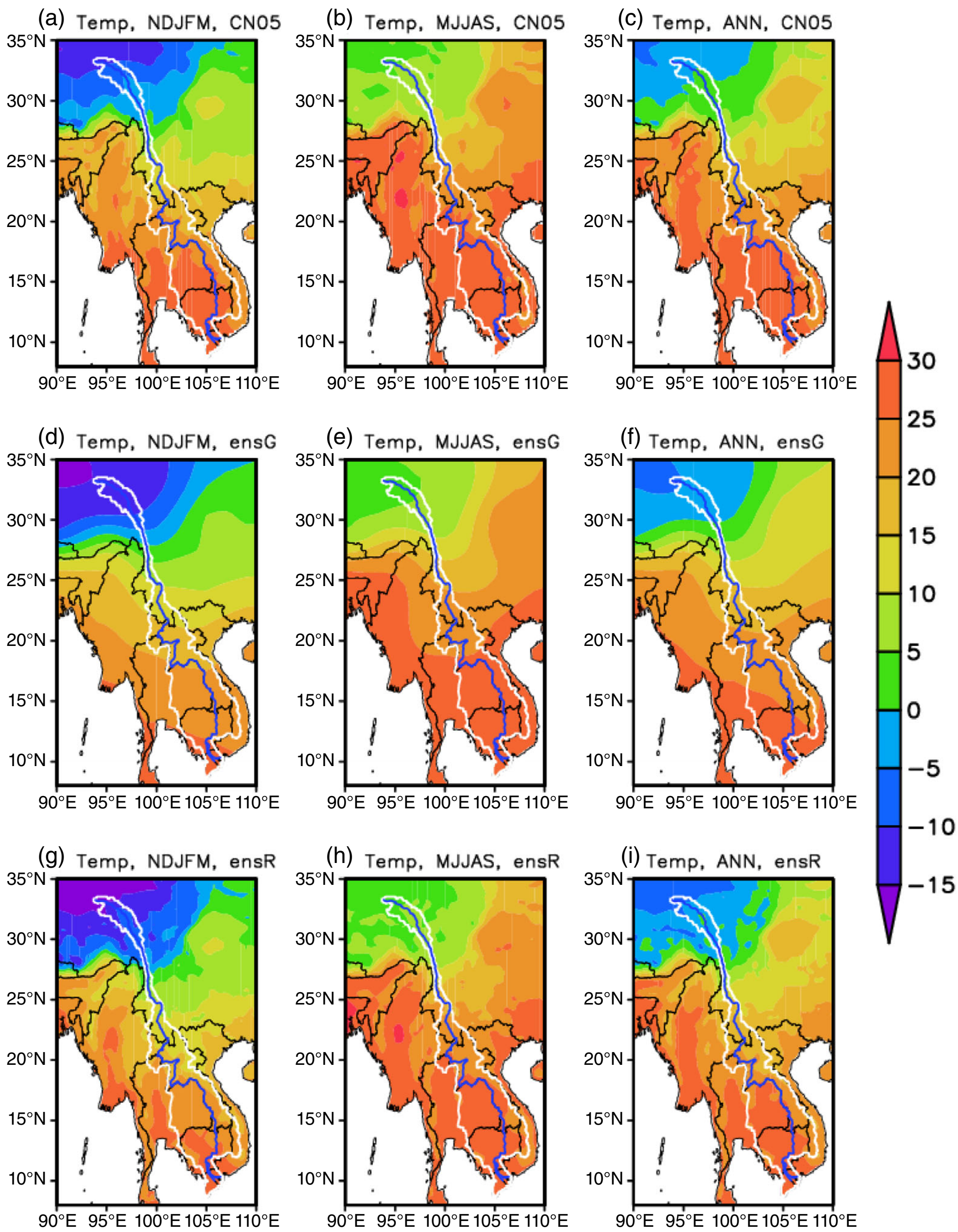

FIGURE 2 Distribution of the present day (1995–2014) temperature. Observation in the dry season (a), the wet season (b), and the whole year (c); simulation by ensemble of GCMs (ensG) in the dry season (d), the wet season (e), and the whole year (f); simulation by ensemble of RegCM4 (ensR) in the dry season (g), the wet season (h), and the whole year (i). Unit: °C

corresponding driving GCM ones are statistically significant only for three out of the five pairs. Thus as found for mainland China (Wu and Gao, 2020), the spatial structure of the temperature biases from the GCMs do not always transfer to the RegCM4, while the internal model physics and especially the effect of high-resolution local topographic forcing play a larger role.

3.2 | Precipitation

In NDJFM the MSEA is generally dry, with less than 150 mm of precipitation over most of the region, except along the coast of Vietnam and over the Malay Peninsula (Figure 4a). The monsoon dominates in the wet season MJJAS, with precipitation greater than 400 mm over most of MSEA, except the northern areas (Figure 4b). Values reaching up to 1,000 mm are found along the west coast of the peninsula, northwestern Myanmar, and portions of southeastern LMRB. The annual mean precipitation follows essentially the wet season one, but with larger values (Figure 4c). The mean precipitation over the LMRB in the dry and wet seasons, and the whole year is 118, 1,018, and 1,342 mm, respectively.

Similar to temperature, the general pattern, magnitude, and seasonal evolution of the observed precipitation

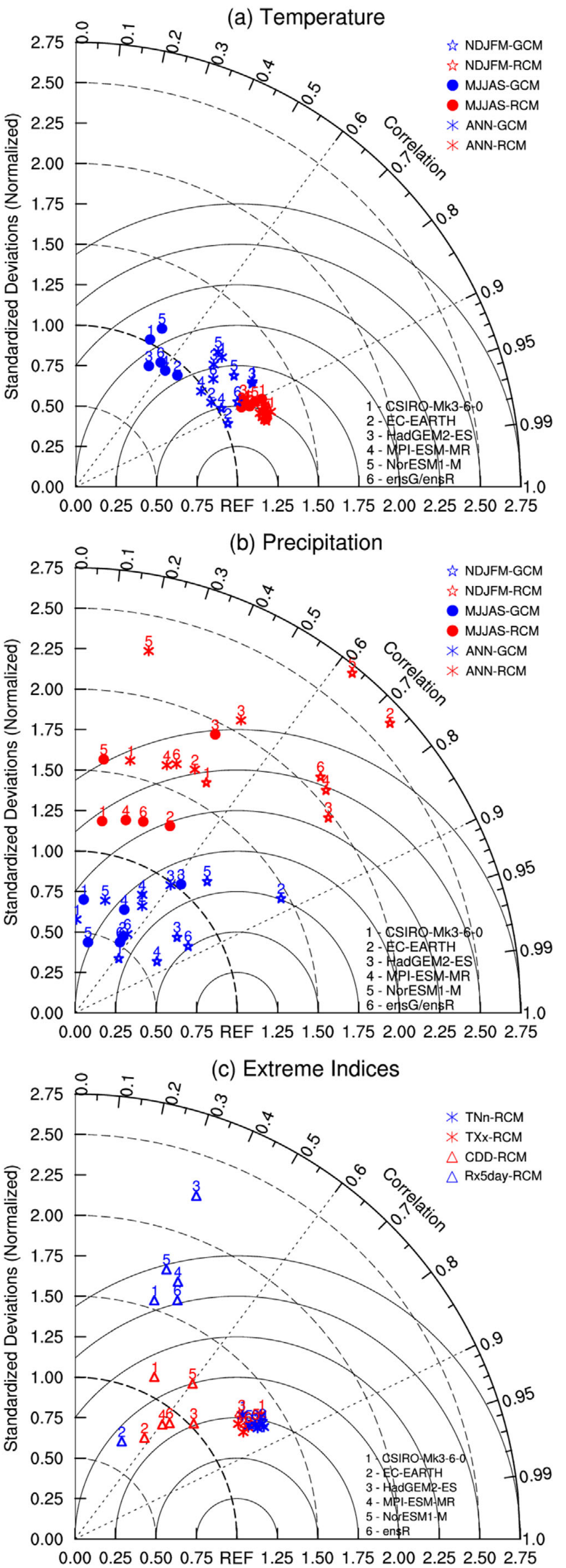

are reproduced quite well by both the ensG and ensR, while ensR provides more regional detail compared to ensG (Figure 4d–i). In fact, the ensR even shows finer spatial structure than the observation dataset, a result not surprising given the sparse distribution of observing sites (Yatagai *et al.*, 2012; Wu and Gao, 2013). For example, the topographical rainfall belt along the mountain chains of the western boarder of Myanmar (Mountain Arakan in the south and Naga Hills in the north) in MJJAS is captured by the ensR but not by APHRODITE, and this may actually be closer to the real precipitation (Figure 4b,h).

A general overestimation of precipitation is found in the model simulations for both seasons and the annual mean, more pronounced in ensR over the mountain areas and the southern edge of the region (figure not shown for brevity). Note that the APHRODITE precipitation may underestimate precipitation over the mountainous areas due to the lack of high-altitude observing sites and the lack of a gauge undercatch correction (e.g., Adam and Lettenmaier, 2003). Regional mean precipitation over the LMRB in the dry and wet seasons, and the whole year are 126, 1,123, and 1,432 mm for ensG, and 182, 1,547, and 1,982 mm for ensR, respectively.

Figure 3b presents the Taylor diagram of precipitation over the MSEA. The spreads are large both for the GCM and RegCM4 ensembles, indicating a large intermodel variability. The spatial correlation coefficients are greater in the dry than the wet season and whole year, for both the GCMs and RegCM4. Greater normalized standard deviation and normalized root-mean-square errors are found for RegCM4, indicating that the RegCM4 produces higher spatial detail than found in the observations.

The CORs of precipitation biases across the model simulations over MSEA are presented in Table 2. The biases across the GCMs are not as consistent as for temperature in NDJFM, with 7 out of 10 CORs being statistically significant, but the CORs are all significant in MJJAS. This indicates a similarity of behaviour across the GCMs. For the RegCM4 simulations, all the CORs are significant, indicating the important role of the internal model physics and processes of the model. This is confirmed by the fact that only three out of five CORs between pairs of GCM-RegCM4 simulation biases are significant.

FIGURE 3 Taylor diagrams of (a) temperature and (b) precipitation over the MSEA between the observations and simulations in GCMs (blue) and RegCM (red) in the dry season (star), the wet season (dot), and the whole year (asterisk) during the present day (1995–2014). (c) Same as (a), but for extreme indices simulated by RegCM

TABLE 1 Spatial correlation coefficients (CORs) of temperature biases in NDJFM (bottom left of the matrix) and MJJAS (top right of the matrix) across the model simulations over MSEA in the present day simulation

	CSIRO	EC	Had	MPI	Nor	CdR	EdR	HdR	MdR	NdR
CSIRO	–	0.90*	0.94*	0.90*	0.96*	0.07	0.40*	0.19	0.37*	0.14
EC	0.79*	–	0.91*	0.85*	0.87*	0.06	0.44*	0.23*	0.43*	0.14
Had	0.81*	0.75*	–	0.91*	0.91*	0.00	0.34*	0.16	0.32*	0.07
MPI	0.84*	0.82*	0.75*	–	0.87*	0.09	0.39*	0.27*	0.36*	0.15
Nor	0.92*	0.70*	0.64*	0.86*	–	0.19	0.47*	0.27*	0.45*	0.25*
CdR	0.19	0.13	−0.18	−0.01	0.23*	–	*0.84**	*0.85**	*0.81**	*0.98**
EdR	0.40*	0.26*	0.11	0.23*	0.46*	*0.86**	–	*0.90**	*0.96**	*0.89**
HdR	0.35*	0.29*	0.07	0.17	0.35*	*0.92**	*0.94**	–	*0.86**	*0.89**
MdR	0.37*	0.28*	0.12	0.20*	0.37*	*0.89**	*0.96**	*0.97**	–	*0.85**
NdR	0.24*	0.14	−0.11	0.05	0.30*	*0.98**	*0.92**	*0.94**	*0.92**	–

Note: Light grey indicates CORs among the GCMs, dark grey for each GCM-RCM pair, and light grey in italic for CORs among the RCM simulations. The asterisks indicate statistically significant at the 95% confidence level.

3.3 | Extreme indices

Figure 5 presents the extreme indices TNn, TXx, CDD, and Rx5day from observations and the ensR simulations (ensG is not shown for brevity and because of the coarse resolution of the GCMs). For the observed TNn (Figure 5a), the lowest temperature values are found over the Tibetan Plateau (<−30.0°C). Above zero temperatures occur over parts of southern China and the Sichuan Basin, and most of the MSEA. The minimum temperatures reach 15.0°C in the southern end of the Peninsula. The spatial pattern of the observed TNn is well reproduced by the ensR, although with a prevailing cold bias (Figure 5b), which is largest (greater than −10.0°C) over the Tibetan Plateau and the surrounding areas, however this result may also be related to the relative paucity of observing stations in high-elevation regions. The bias is much smaller over the eastern part of MSEA (~2.0°C), while a warm bias ~2.0°C over Myanmar and west of it is found. Regional mean values of TNn in LMRB from the observation and ensR are 7.6 and 3.3°C, respectively.

The values of TXx (Figure 5c,d) range from 30.0 to 35.0°C over most of the analysis region except for the Tibetan Plateau. Cold biases >5.0°C still exist in the southern part of the Tibetan Plateau, and warm biases of up to 5.0°C are found over the centre of Sichuan Basin in China and portions west of Myanmar. A mix of cold and warm biases within ±2.0°C is found over most of MSEA. Regional mean values of TXx in LMRB are 35.5 and 34.5°C for the observations and ensR, respectively.

The observed CDD shows the smallest values (30 days) along the east coast of MSEA and the southeastern part of China (Figure 5e). Values in excess of 60 days are located over the Central Myanmar Basin (the Irrawaddy River valley), northwest boundary of the analysis region over the Tibetan Plateau, and western part of the Yunnan Province in China. The general CDD spatial pattern and low values in the Central Myanmar Basin are well reproduced in ensR (Figure 5f), but with a prevailing underestimation, likely due to the occurrence of too many drizzle days. In LMRB, the observed regional mean of CDD is 46 days, while it is 30 days in ensR.

The Rx5day show a strong topographic dependence, with large values greater than 150 mm mostly along the mountain ranges in the west coast and the border areas of Vietnam and Laos, as well as in the southern slope of the Himalayas (Figure 7g). The topographic effect in ensR is more pronounced, characterized by greater values, and larger areas across the mountains (Figure 5h). Finer spatial detail in ensR compared to the observation is also evident, consistently with the average precipitation. The mean over LMRB for ensR is 177 mm, compared to 114 mm in the observations, thus illustrating a pronounced over prediction, which however, as mentioned earlier, may be amplified by deficiencies in the observations.

Figure 3c shows the Taylor diagram for the extreme indices. The temperature extreme indices are well reproduced by RegCM4 with a small spread among the simulations, and the values of spatial correlation coefficients, normalized standard deviation, and centred root-mean-square errors are around 0.85, 1.25, and 0.75, respectively. A larger spread is found for CDD, with the spatial correlation coefficients around 0.60, normalized standard deviation ranging from 0.75 to 1.25, and the centred root-mean-square errors in the range of 0.75–1.00. For Rx5day, the spatial correlation coefficients are lower compared to the other indices, with the values ranging

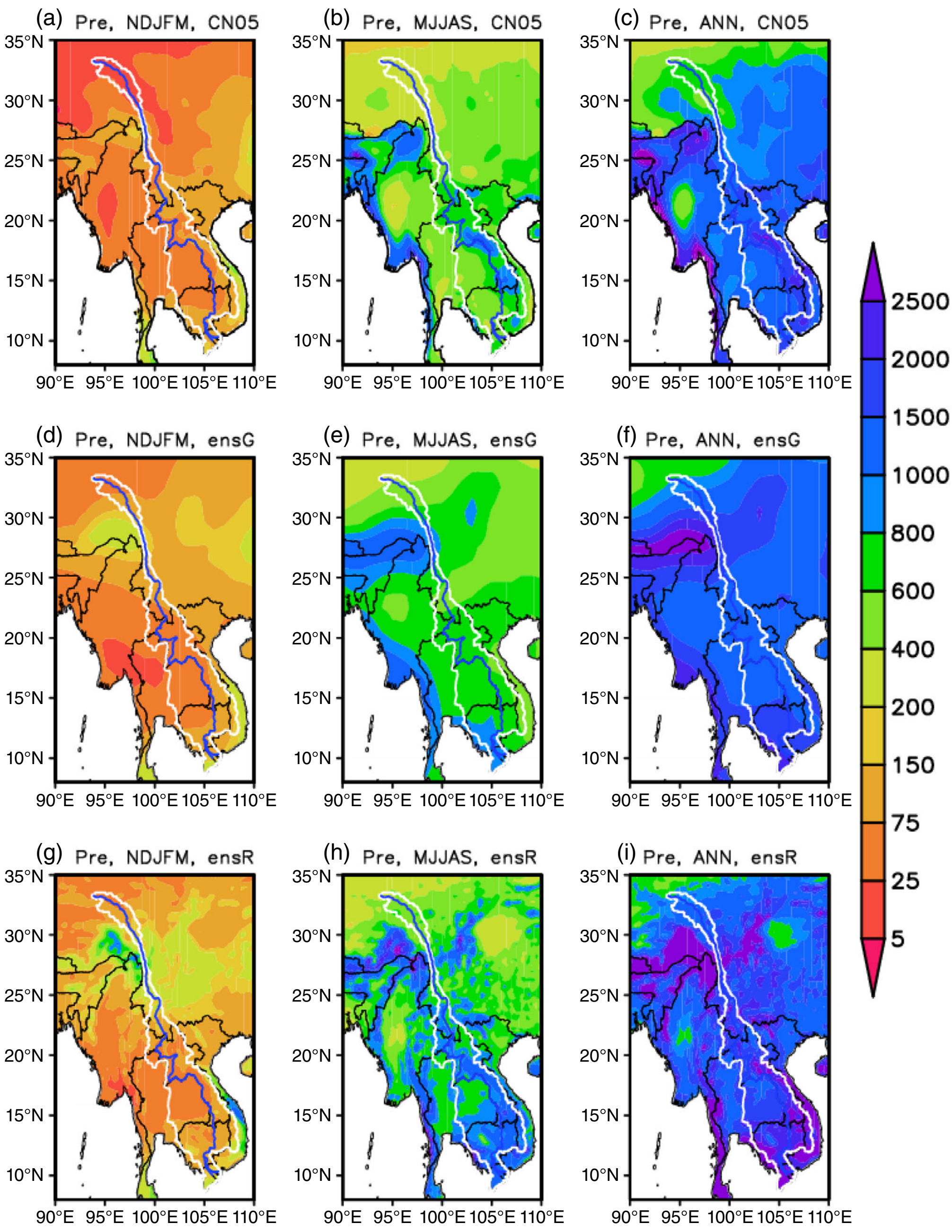

FIGURE 4 Same as Figure 2, but for precipitation. Unit: mm

from 0.30 to greater than 0.40. The normalized standard deviation are mostly greater than 1.50, except for the EC-EARTH driven run.

4 | FUTURE CHANGES

4.1 | Temperature

Figure 6 shows the projected temperature change over the MSEA by the end of the 21st century. Substantial warming is found in the future over the region, more pronounced in NDJFM compared to MJJAS and in the northern regions compared to the southern ones. In NDJFM, the warming projected by ensG is evenly distributed, with values greater than 2.4°C over most of the analysis region (Figure 6a), while in ensR the warming shows large subregional variability, with values >3.0°C over the Tibetan Plateau at high altitudes, and <2.0°C over the Peninsula (Figure 6d). This warming amplification effect with elevation, mostly in response to a reduction of snow cover, has been found in previous work (e.g., Giorgi *et al.*, 1997; Jiang and Fu, 2012; Fu *et al.*, 2021). The regional mean warming values over LMRB for the ensG and ensR under RCP4.5 are 2.3°C (with 1.4–3.6°C intermodel spread), and 1.9°C (0.7–

TABLE 2 Same as Table 1, but for precipitation biases

	CSIRO	EC	Had	MPI	Nor	CdR	EdR	HdR	MdR	NdR
CSIRO	–	0.69*	0.55*	0.75*	0.82*	0.43*	0.38*	0.09	0.39*	0.39*
EC	−0.11	–	0.64*	0.77*	0.83*	0.55	0.40*	0.11	0.51*	0.51*
Had	0.81*	−0.19	–	0.61*	0.45*	0.13	0.21*	0.05	0.22*	0.14
MPI	0.88*	−0.08	0.82*	–	0.85*	0.50*	0.51*	0.24*	0.57*	0.52*
Nor	0.64*	0.30*	0.56*	0.66*	–	0.65*	0.50*	0.20*	0.60*	0.61*
CdR	0.34*	0.24*	0.15	0.22*	0.40*	–	0.72*	0.47*	0.79*	0.96*
EdR	−0.25*	0.65*	−0.39*	−0.33*	0.09	0.67*	–	0.72*	0.88*	0.79*
HdR	−0.11	0.44*	−0.22*	−0.10	0.28*	0.78*	0.85*	–	0.73*	0.59*
MdR	−0.01	0.50*	−0.16	−0.08	0.27*	0.86*	0.92*	0.92*	–	0.86*
NdR	0.00	0.49*	−0.16	−0.08	0.27*	0.90*	0.91*	0.87*	0.97*	–

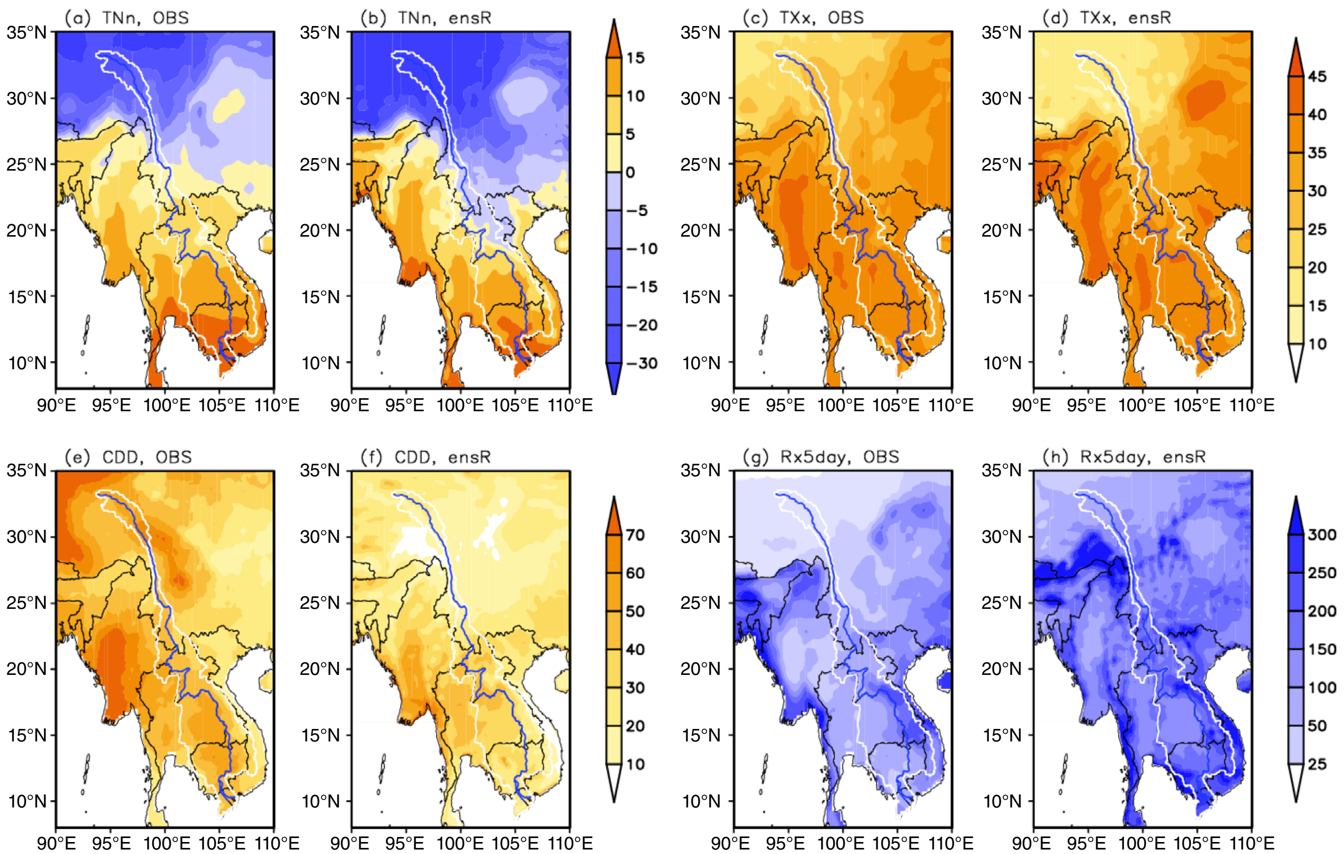

FIGURE 5 Distribution of present day (1995–2014) TNn (a), TXx (c), CDD (e), and Rx5day (g) in observations; simulation of TNn (b), TXx (d), CDD (f), and Rx5day (h) by ensemble of RCMs (ensR). Units are: °C, °C, day, and %, respectively

2.7°C), respectively (Table 3). Therefore, lower region-average warming and intermodel spread are found for RegCM4, the latter result likely due to the use of the same physics schemes in all runs, which modulate the effect of the lateral boundary forcing.

The warming is lower during the wet season MJJAS (Figure 6b,e) for both ensG and ensR. Again, a general lower warming is simulated in ensR compared to ensG. In ensG, minimum warming values smaller than 1.8°C occur along the western and southern coasts of the peninsula, while larger values occur in the northeastern portions of the region (2.1–2.4°C, Figure 6b). For ensR, the temperature increase is lower than 1.4°C over most of the peninsula, and the largest increase ranges from 2.1 to

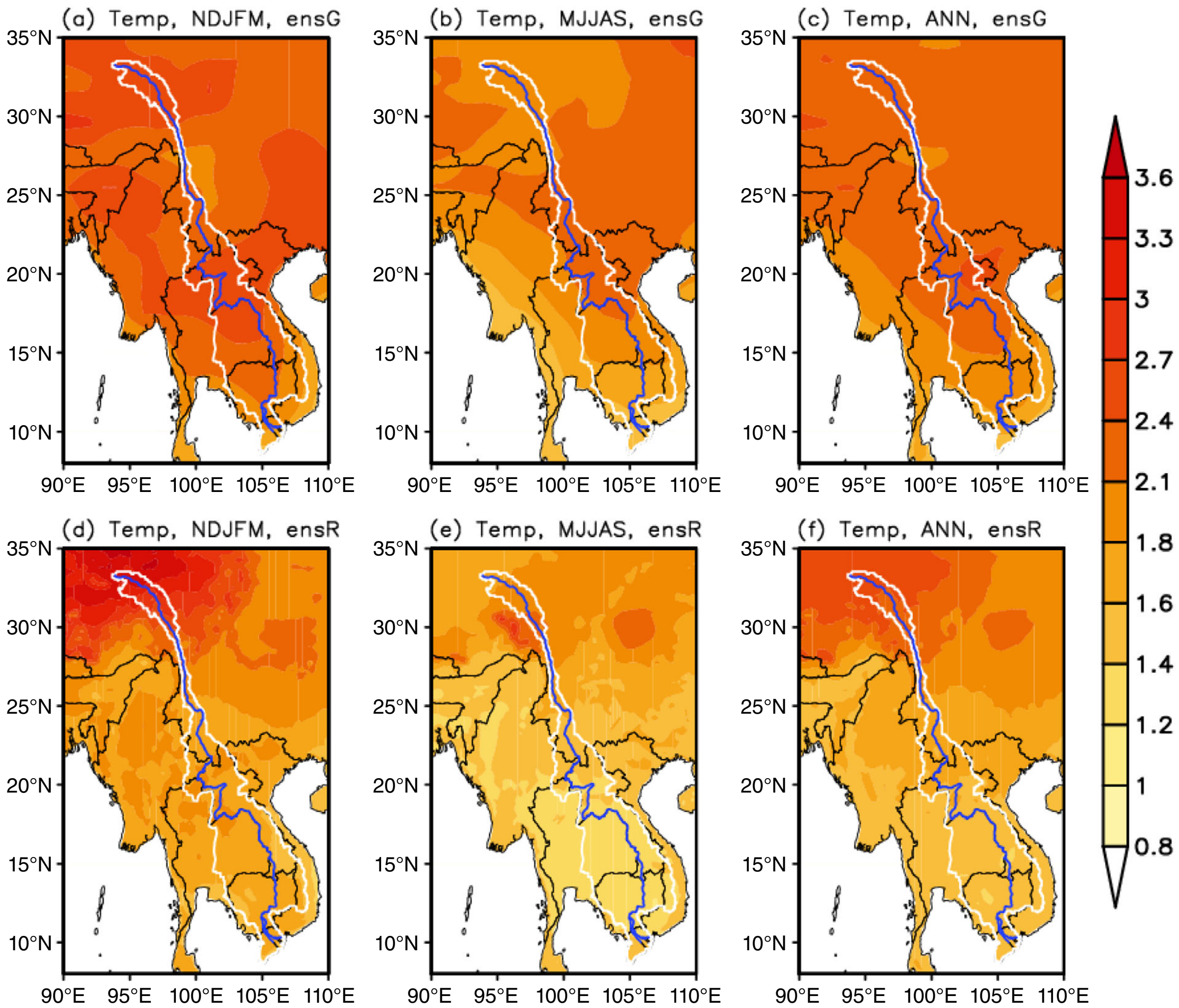

FIGURE 6 The projected changes of temperature at the end of 21st century (2079–2098) relative to the present day under RCP4.5 pathway. By ensG in the dry season (a), the wet season (b), and the whole year (c); by ensR in the dry season (d), the wet season (e), and the whole year (f). The sign of the change show good agreements for the intermodels and cross simulations, thus not shown for brevity. Unit: °C

TABLE 3 Projected regional mean changes in NDJFM, MJJAS, and annual mean temperature and precipitation over Lancang-Mekong River basin by both ensG and ensR in the mid- (2041–2060) and end (2079–2098) of the 21st century relative to the present day (1995–2014) under RCP4.5 and RCP8.5

Variables	Periods	RCPs	NDJFM (ensG/ensR)	MJJAS (ensG/ensR)	ANN (ensG/ensR)
Temp. (°C)	Mid	RCP4.5	1.5/1.3 (0.9–2.3/0.7–1.7)	1.3/0.9 (1.1–1.6/0.5–1.5)	1.4/1.1 (1.1–1.9/0.9–1.6)
		RCP8.5	2.0/1.8 (1.3–2.8/1.4–2.1)	1.7/1.4 (1.4–2.2/1.0–1.8)	1.9/1.6 (1.4–2.4/1.3–2.0)
	End	RCP4.5	2.3/1.8 (1.4–3.6/0.7–2.7)	1.9/1.6 (1.4–2.5/1.3–2.2)	2.1/1.6 (1.4–3.0/1.1–2.4)
		RCP8.5	4.2/3.5 (3.2–5.6/2.3–4.5)	3.8/3.2 (3.2–4.9/2.7–3.8)	4.0/3.4 (3.2–5.0/2.5–4.1)
Prep. (%)	Mid	RCP4.5	5/4 (−10–30/−3–12)	2/−2 (−2–7/−4–1)	3/1 (−2–7/−2–3)
		RCP8.5	1/1 (−25–16/−7–12)	3/−3 (−1–6/−6–1)	3/−1 (−1–7/−5–2)
	End	RCP4.5	7/7 (−18–30/−4–14)	4/0 (−3–9/−5–7)	6/1 (2–12/−2–6)
		RCP8.5	14/4 (−24–44/−17–28)	9/2 (−4–18/−6–12)	11/2 (3–20/−4–15)

Note: The values in brackets are the minimum and maximum in the five models/simulations.

TABLE 4 Spatial correlation coefficients (CORs) of changes in temperature in NDJFM (bottom left of the matrix) and MJJAS (top right of the matrix) across the model simulations over the MSEA in the end of the 21st century (2079–2098) relative to the present day (1995–2014) under RCP8.5

	CSIRO	EC	Had	MPI	Nor	CdR	EdR	HdR	MdR	NdR
CSIRO	–	0.84*	0.53*	0.84*	0.87*	0.75*	0.59*	0.50*	0.86*	0.70*
EC	0.25*	–	0.65*	0.89*	0.89*	0.67*	0.41*	0.28*	0.70*	0.61*
Had	0.58*	0.73*	–	0.63*	0.66*	0.69*	0.00	0.28*	0.35*	0.10
MPI	0.49*	0.73*	0.54*	–	0.97*	0.64*	0.53*	0.30*	0.76*	0.73*
Nor	0.40*	0.53*	0.65*	0.59*	–	0.72*	0.57*	0.41*	0.79*	0.71*
CdR	0.61*	0.00	0.05	0.34*	0.16	–	*0.49**	*0.70**	*0.75**	*0.44**
EdR	0.18	0.80*	0.75*	0.50*	0.63*	*0.05*	–	*0.64**	*0.78**	*0.84**
HdR	−0.07	0.76*	0.49*	0.47*	0.37*	*−0.10*	*0.81**	–	*0.62**	*0.39**
MdR	0.19	0.87*	0.62*	0.69*	0.47*	*0.17*	*0.87**	*0.78**	–	*0.80**
NdR	−0.30*	0.53*	0.42*	0.22*	0.54*	*−0.41**	*0.66**	*0.65**	*0.50**	–

Note: Light grey indicates CORs among the GCMs, dark grey for each GCM-RCM pair, and light grey in italic for CORs among the RCM simulations. The asterisks indicate statistically significant at the 95% confidence level.

2.4°C only over small areas along 30°N in the north (Figure 6e). The region-mean warming over the LMRB for ensG and ensR under RCP4.5 is 1.9°C (1.4–2.5°C) and 1.4°C (1.0–2.2°C), respectively.

The magnitude and distribution of the projected changes in annual mean temperature lie between those for the dry and wet season (Figure 6c,f). In ensG, the warming is evenly distributed over the region, mostly ranging from 2.1 to 2.4°C (Figure 6c). In ensR, the warming is greater in the north, with the largest values >2.4°C over the Tibetan Plateau, and lower in the south, in the range of 1.4–1.6°C over the MSEA (Figure 6f). The projected mean changes in annual temperature over the LMRB in ensG and ensR are 2.1°C (1.5–3.0°C) and 1.6°C (1.0–2.4°C) under RCP4.5, and 4.0°C (3.5–5.0°C) and 3.4°C (2.5–4.1°C) under RCP8.5, respectively.

It is noted that the relatively low warming by the RegCM4 compared to the driving GCMs was also found over China by Wu and Gao (2020), and this result was found also in other RCMs (Olson *et al.*, 2016; Tang *et al.*, 2016; Sørland *et al.*, 2018). It is difficult to identify the reasons for this behaviour, as it may depend on many processes. For example, Sørland *et al.* (2018) argue that in summer, warm model biases may lead to stronger warming due to land surface feedback, whereby lower warming found in RCMs is related to their lower warm biases. In our case the biases of the GCM and RCM are more consistent except for regional details, and therefore this may not be a primary mechanism. The simulation of clouds and transfer processes in the boundary layer may provide additional contributions, and further analysis is needed to better address the different behaviours of ensR and ensG over the MSEA region.

The regional mean warming and the intermodel/simulation spreads of ensG and ensR over the LMRB at the mid- and end of the 21st century under the RCP4.5 and RCP8.5 are shown in Table 3. The changes at the mid-21st century show similar behaviour as at the end of century, with greater warming in NDJFM compared to MJJAS, and ensG compared to ensR, but with smaller values compared to the end of century. Consistently, the temperature increases show greater values for the high-level RCP8.5 than the mid-level RCP4.5. By the end of the century, the magnitude of the warming is almost doubled in RCP8.5 compared to RCP4.5.

The CORs of temperature change by the end of 21st century under RCP8.5 across the model simulations over the MSEA are presented in Table 4, where the high-level RCP8.5 is used to maximize the signal to noise ratio. The CORs across the GCMs are all statistically significant in both NDJFM and MJJAS, with greater values for MJJAS. The CORs for each pair of the GCM-RegCM4 are all significant in both seasons, indicating the large forcing from the driving field. However, a larger spread of the temperature change pattern is found for RegCM4, with the CORs being significant in 7 out of 10 cases in NDJFM and 9 out of 10 in MJJAS.

4.2 | Precipitation

Precipitation changes by the end of 21st century are presented in Figure 7, along with the wind changes at 700 hPa. For ensG in NDJFM, a prevailing increase is found over the region (Figure 7a), mostly greater than 10%, with maxima reaching >25%. Small changes ranging from −5 to 5% are found over southern Vietnam. The

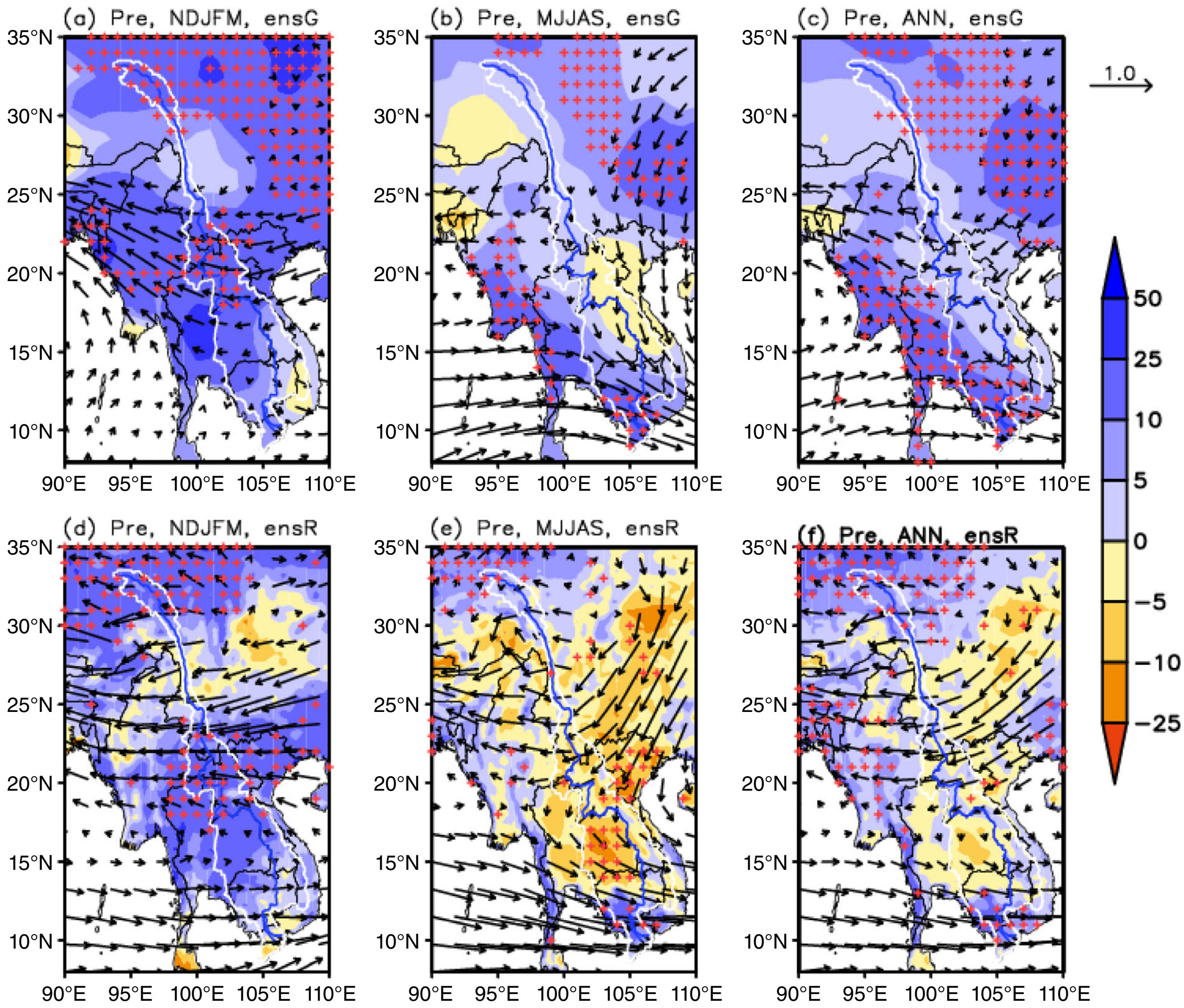

FIGURE 7 Same as Figure 5, but for precipitation change and the arrows indicating horizontal wind change at 700 hPa. The cross indicates at least four out of five models/simulations agree on the sign of change. Units: % and m·s^{-1}

increase is also small, mostly <10%, along the areas between 25°N and 30°N and west of 105°E. The intermodel agreement in the sign of change is high over the northeastern and central portions of the region, with pronounced increases there.

A general increase in precipitation is also found for ensR over most of MSEA, with good cross-simulation agreement over the Tibetan Plateau in the northwest, and in the northern part of the MSEA (Figure 7d). Meanwhile, decreases of up to −5 to −10% are found over the area extending from the western coast of Myanmar to the Sichuan Basin in China (around 27.5°N, 105°E), although in these areas there is poor cross-simulation agreements. Regional mean precipitation changes for ensG and ensR over the LMRB under RCP4.5 are 9% (−16 to +33%) and 7% (−3 to +15%), respectively (Table 3).

During the wet season (MJJAS), precipitation mostly increases in ensG, with the largest increase, greater than 10%, occurring over the west coast of MSEA and Guangxi-Guizhou areas in southern China (Figure 7b). Slight decreases (<5%) are found over Laos and northern Vietnam, the southern part of the Tibetan Plateau, and the border areas of Bangladesh-India-Myanmar in the northwest coast of MSEA. The models agree well over the places with large increases (>5%).

Conversely, the projected precipitation in ensR shows a general decrease over the region, with good agreement among the places with large values (~−10%) (Figure 7e). The largest decrease in the range of −10 to −15% is mainly found in northern Vietnam and southeastern Thailand. While the regional mean change over the LMRB is positive, 4% (−4 to +9%), in ensG, it is negative, −2% (−5 to 0%) in ensR (Table 3) under RCP4.5. In general, the annual mean precipitation change pattern projected in ensG and ensR are consistent with the values in the wet season MJJAS but with lower magnitudes

TABLE 5 Same as Table 4, but for changes in precipitation

	CSIRO	EC	Had	MPI	Nor	CdR	EdR	HdR	MdR	NdR
CSIRO	–	0.60*	−0.04	0.63*	0.16	0.27*	0.36*	0.41*	0.33*	0.37*
EC	−0.70*	–	0.32*	0.67*	0.03	0.49*	0.50*	0.33*	0.38*	0.42*
Had	−0.50*	0.52*	–	0.29*	0.12	0.03	0.11	0.31*	0.11	0.09
MPI	0.55*	−0.54*	−0.65*	–	0.06	0.31*	0.48*	0.30*	0.30*	0.34*
Nor	−0.83*	0.76*	0.57*	−0.68*	–	−0.16	−0.12	−0.09	−0.27*	−0.24*
CdR	0.70*	−0.67*	−0.56*	0.57*	−0.65*	–	*0.73**	*0.30**	*0.70**	*0.53**
EdR	−0.38*	0.45*	0.30*	−0.02	0.33*	*−0.41**	–	*0.60**	*0.80**	*0.63**
HdR	−0.12	0.45*	0.37*	−0.13	0.23*	*−0.23**	*0.59**	–	*0.61**	*0.54**
MdR	0.58*	−0.66*	−0.76*	0.74*	−0.70*	*0.75**	*−0.33**	*−0.44**	–	*0.67**
NdR	−0.62*	0.78*	0.64*	−0.52*	0.69*	*−0.78**	*0.59**	*0.63**	*−0.81**	–

(Figure 7c,f). The regional mean changes of annual mean precipitation over the LMRB for ensG and ensR are 6% (+2 to +13%) and 1% (−2 to +4%) under RCP4.5, and 11% (+3 to +20%) and 2% (−4 to +15%) under RCP8.5, respectively (Table 3).

The differences of precipitation changes between ensG and ensR may attribute to the stronger topographic forcing and the better resolution of the monsoon dynamics and small scale weather and climate systems in the RegCM4 (e.g., Gao *et al*., 2006; 2012). As shown in Figure 7a, in NDJFM the ensG, with a smoothed topography, simulates a small change in the wind field over the Sichuan Basin. Conversely, in ensR, an anticyclonic circulation, and a reinforced westward flow south and west of the basin are evident (Figure 7d). These lead to the increase of precipitation in ensG but a decrease in ensR over the areas.

In MJJAS, a northeast wind change is found in ensG over the Sichuan Basin, turning towards the north over the eastern part of the Indochina Peninsula. This leads to the increase of precipitation over the Basin and a slight decrease over the eastern part of the Peninsula (Figure 7b). In ensR, the wind circulates around the mountain chains east of the Basin and then turns towards a southwest direction in the northern part of the Peninsula (Figure 7e), turning to the southeast direction as forced by the Mountain Bilauktaung in the western boundary of Thailand. An intensified anticyclonic circulation is then formed over the Indochina peninsula, leading to decreased precipitation there in ensR.

The regional mean changes in precipitation and the intermodel spreads across the ensG and ensR ensembles over the LMRB at the mid- and end of the 21st century under the RCP4.5 and RCP8.5 scenarios are presented in Table 3. In the ensG RCP4.5, the projected regional mean changes during the mid-21st century are about half as large as those found at the end of the century. Closer values of the change between the mid- and end of the century are found for ensR in MJJAS and the whole year. Under the RCP8.5, a continuous increase in precipitation is found throughout the century in ensG, with the magnitude of the change at the end of the century doubled compared to RCP4.5. The NDJFM/MJJAS/annual mean increases in the mid- and end of the century under the RCP4.5 and RCP8.5 in ensG are 1/3/3% and up to 14/9/11%, respectively. The regional mean changes are much weaker in ensR due to the presence of broad areas of decrease (Figure 7d–f).

The CORs for the precipitation changes by the end of 21st century under RCP8.5 across the model simulations are presented in Table 5. For the GCMs, almost no consistency is found across the change patterns, in particular for NDJFM, even with of negative COR values. The driving from the GCM is evident in RegCM4 simulations, with most of the GCM/RegCM4 CORs being significant (except Nor-NdR in MJJAS). For the cross correlations across the RegCM4 runs, less than half of the cases for NDJFM, but 8 out 10 cases for MJJAS show positive COR values, indicating that the change signal is more consistent in the wet than the dry season.

4.3 | Extreme indices

Figure 8a,b shows the spatial distributions of the projected changes in TNn and TXx by the end of 21st century from ensR under RCP4.5. Significant increases of both TNn and TXx are found under warming conditions, indicating fewer cold events and more heat waves in the future. For TNn, the increases are more pronounced over the high-latitude and high-altitude areas, particularly over the Tibetan Plateau, with the values of increase greater than 3.5°C (Figure 8a). This is likely due to the reduction of snow cover and the snow albedo feedback effect. The increase is much lower, in the range of 1.0–

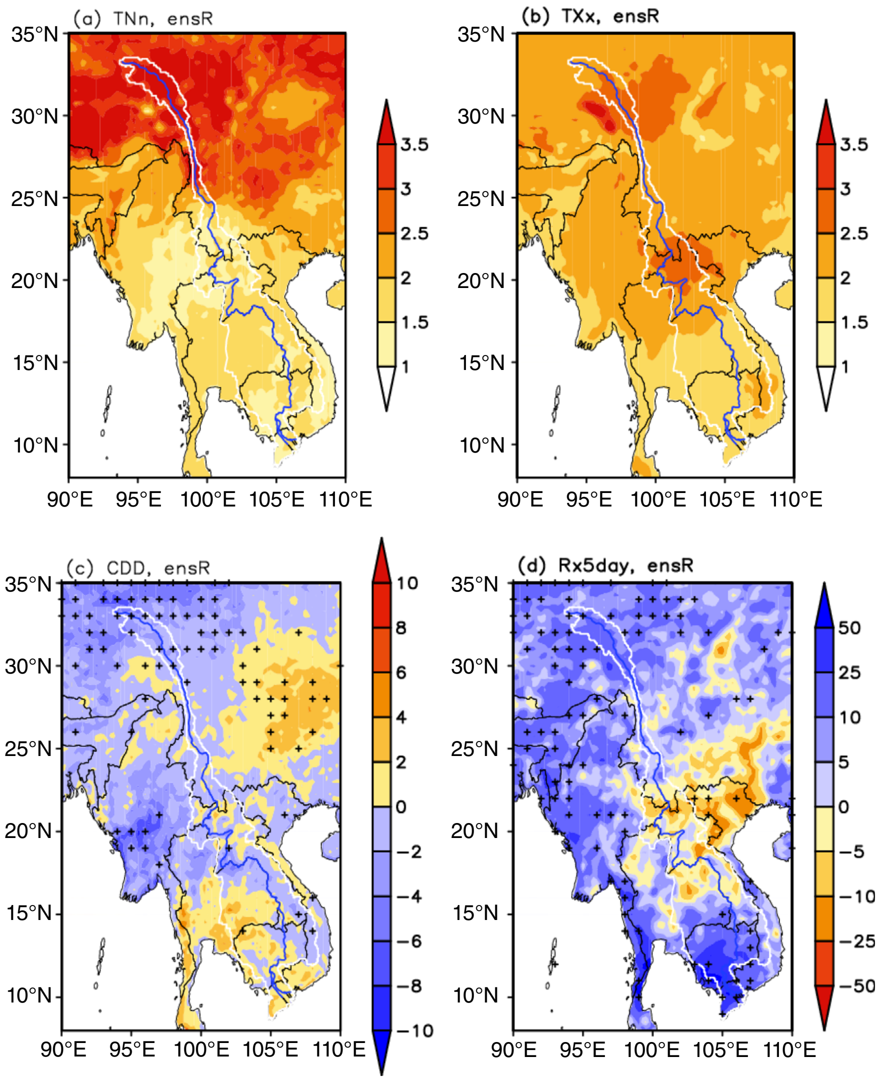

FIGURE 8 The projected changes of TNn (a), TXx (b), CDD (c) and RX5day (d) at the end of 21st century in ensR. The cross indicates at least four out of five models/simulations agree on the sign of change. Units are: °C, °C, day, and %, respectively

TABLE 6 Projected regional mean changes in TNn, TXx, CDD, and Rx5day over Lancang-Mekong River basin by ensR in the mid (2041–2060) and end (2079–2098) of the 21st century relative to the present day (1995–2014) under RCP4.5 and RCP8.5

Periods/variable	RCPs	TNn (°C)	TXx (°C)	CDD (day)	Rx5day (%)
Mid	RCP4.5	1.3 (1.1–1.8)	1.5 (1.1–2.0)	0.4 (−0.8–1.8)	5.6 (0.2–14.5)
	RCP8.5	2.0 (1.7–2.2)	2.0 (1.6–2.6)	−0.1 (−0.2–2.4)	4.8 (2.2–9.4)
End	RCP4.5	1.8 (0.9–2.6)	2.1 (1.7–2.9)	−0.3 (−1.8–1.4)	8.4 (−1.1–16.8)
	RCP8.5	4.1 (3.4–4.9)	4.2 (3.4–4.9)	−0.4 (−3.6–2.7)	16.5 (10.3–22.3)

Note: The values in brackets are the minimum and maximum in the five models/simulations.

2.0°C, towards the south over most parts of the MSEA. The increases for TXx are more evenly distributed (Figure 8b), with values mostly greater than 2.0°C north of 15°N, and lower than 2.0°C in southern regions. Regional mean changes of TXx and TNn over the LMRB under RCP4.5 are 1.8°C (0.9–2.6°C) and 2.1°C (1.7–2.9°C), and to a much greater extent under RCP8.5 as 4.1°C (3.4–4.9°C), 4.2°C (3.4–4.9°C), respectively (Table 6).

Changes in CDD and Rx5day at the end of the 21st century are presented in Figure 8c,d, respectively. For CDD, an increase with good cross-simulation agreement is found over a broad area extending from the Sichuan Basin to the Yunnan Provinces in southwest China, with increases in the range of 2–4 days (∼10–25%) in correspondence of prevailing precipitation decreases in both the dry and wet season (Figure 7). Prevailing increases in CDD are also found over southwestern MSEA, including southern Thailand, most of Cambodia, and southern Vietnam, although with low intersimulation agreements. Regional mean changes of CDD under RCP4.5 and RCP8.5 over LMRB are −0.3 day (−1.8 to +1.4 day) and 8.4% (−1.1 to +16.8%), respectively (Table 6).

The Rx5day is projected to increase over most of the analysis region, except in the border areas from southwest China to northern Vietnam and Laos, and the mid-reaches of the LMRB (Figure 8d). The increase is mostly in the range of 10–25%, with good cross-simulation agreement over the Tibetan Plateau, the western part of MSEA, and the lower reaches of the LMRB. Comparison with Figure 8c shows that increases in both CDD and Rx5day are found over southwestern China and the lower reaches of LMRB, suggesting greater risk of both flood and drought events. Regional mean change over LMRB under RCP4.5 is 8.4% (−1.1 to +16.8%) and almost doubled under RCP8.5, being 16.5% (+10.3 to +22.3%) (Table 6).

5 | CONCLUSIONS AND DISCUSSIONS

We evaluated the simulations of present-day climate (1995–2014) and projected future changes at the mid- and end of the 21st century (2041–2060 and 2079–2098) over the MSEA region based on an ensemble of RegCM4 simulations under the RCP4.5 and RCP8.5 pathways, driven by different CMIP5 GCMs. We found that the RCM simulations provide more realistic spatial details of present day distributions of both temperature and precipitation compared to the driving GCMs, with the latter reproducing only the broad patterns of these variables. The topographic effect on precipitation is well described by ensR, particularly for extremes as measured by the Rx5day index. A general cold and wet bias prevails in both the GCMs and RegCM4 in all seasons.

In general, the biases for temperature and precipitation show consistent spatial patterns within the GCMs and RegCM4 simulation ensembles, except for precipitation during dry season. However, weak correlations between the biases in the GCMs and the nested RegCM4 are found, indicating the important role of the internal model physics and processes of the regional model.

Significant warming is projected by both ensG and ensR in all seasons and the annual mean. Large differences are found in the spatial distribution and magnitude of warming between ensG and ensR, with more regional details in ensR. The warming in ensR is about half a degree lower than in ensG for all seasons in the LMRB. The regional mean annual temperature increases over the LMRB for ensG and ensR are 2.1 and 1.6°C, respectively, under RCP4.5 by the end of 21st century. The changes under RCP8.5 are in a greater extent compared to RCP4.5.

The spatial pattern of the projected changes in precipitation show large spreads across the GCM ensemble, and the RegCM4 one in NDJFM, while the change patterns in the RegCM4 are generally consistent with the driving GCM ones. However differences in the ensemble mean changes between the GCM and RegCM4 ensembles are found, particularly in the wet season, with a general increase of precipitation in ensG and broad areas of decrease in ensR (as also reported by Tangang *et al.*, 2020). For the regional mean over the LMRB, the change is 4% for ensG, but −2% for ensR, respectively, under RCP4.5 by the end of 21st century.

These differences may be associated with the stronger topographic forcing and the related circulation changes in RegCM4, although further experiments and analysis are indeed needed to better understand the model behaviours and physical mechanisms behind these results.

The changes of the extreme indices, TNn and TXx for temperature, and CDD and Rx5day for precipitation, as projected by RegCM4 indicate general increases of the temperature extreme indices TNn and TXx, that is, future decreases of cold spells and increase of heat waves in the region; and a prevailing increase of Rx5day and, longer CDD in the northeast and southwest of the MSEA, that is, increases of both wet and dry extremes. Over the LMRB under RCP4.5, we find an increase of 1.8°C for TNn and 2.1°C for TXx, along with an 8.4% increase of Rx5day by the end of 21st century.

While our results are potentially valuable for the better understanding of future climate changes and the uncertainties related over the region, the data are also available to support impact models, for example, hydrology and water resources, agriculture, and ecosystem models, for the further assessments of the impacts and the possible implementation of proper adaptation measures.

Finally, here we have used only one RCM, and the model was customized based on a performance analysis over China, although driven by a range of GCMs, and good cross-simulation agreement was found over areas with larger changes. Future studies should employ multi-GCM/RCM ensembles and high model resolution over this region with complex topography in order to better characterize uncertainties in projections over the region. We plan to conduct a comparison with the results from other possible RCMs, in particular those from CORDEX-SEA project (Tangang *et al.*, 2020), and to carry out new simulations driven by the new generation CMIP6 global climate projections.

AUTHOR CONTRIBUTIONS

Yuanhai Fu: Formal analysis; funding acquisition; investigation; methodology; validation; visualization; writing – original draft; writing – review and editing. **Xuejie Gao**: Conceptualization; funding acquisition; project administration; resources; supervision; writing – original draft; writing – review and editing. **Ying Xu**: Investigation; writing – original draft; writing – review and editing. **Filippo Giorgi**: Investigation; writing – original draft; writing – review and editing.

ACKNOWLEDGEMENTS

This research was supported by the Strategic Priority Research Program of the Chinese Academy of Sciences (XDA2006040102), the National Natural Science Foundation of China (41675103), and the Science and Technology Program of Yunnan (2018BC007).

ORCID

Yuanhai Fu https://orcid.org/0000-0001-8162-4840
Filippo Giorgi https://orcid.org/0000-0003-2895-5274

REFERENCES

Adam, J.C. and Lettenmaier, D.P. (2003) Adjustment of global gridded precipitation for systematic bias. *Journal of Geophysical Research: Atmospheres*, 108, 4257–4268. https://doi.org/10.1029/2002JD002499.

Bentsen, M., Bethke, I., Debernard, J., Iversen, T., Kirkevåg, A., Seland, Ø., Drange, H., Roelandt, C., Seierstad, I., Hoose, C. and Kristjánsson, J. (2013) The Norwegian earth system model, NorESM1-M—Part 1: description and basic evaluation of the physical climate. *Geoscientific Model Development*, 6, 687–720. https://doi.org/10.5194/gmd-6-687-2013.

Chhin, R., Oeurng, C. and Yoden, S. (2020) Drought projection in the Indochina region based on the optimal ensemble subset of CMIP5 models. *Climatic Change*, 162, 687–705. https://doi.org/10.1007/s10584-020-02850-y.

Christensen, J.H., Hewitson, B., Busuioc, A., Chen, A., Gao, X., Held, I., Jones, R., Kwon, W., Laprise, R., Magaña, V., Mearns, L., Menendez, C., Räisänen, J., Rinke, A., Kolli, R.K., Sarr, A. and Whetton, P. (2007) Regional climate projections. In: Solomon, S., Qin, D., Manning, M., Chen, Z., Marquis, M., Averyt, K.B., Tignor, M. and Miller, H.L. (Eds.) *Climate Change 2007: The Physical Science Basis. Contribution of Working Group I to the Fourth Assessment Report of the Intergovernmental Panel on Climate Change*. Cambridge and New York, NY: Cambridge University Press.

Collins, W.J., Bellouin, N., Doutriaux-Boucher, M., Gedney, N., Halloran, P., Hinton, T., Hughes, J., Jones, C.D., Joshi, M., Liddicoat, S., Martin, G., O'Connor, F., Rae, J., Senior, C., Sitch, S., Totterdell, I., Wiltshire, A. and Woodward, S. (2011) Development and evaluation of an Earth-System model-HadGEM2. *Geoscientific Model Development*, 4, 1051–1075. https://doi.org/10.5194/gmd-4-1051-2011.

Fan, H. and He, D. (2015) Temperature and precipitation variability and its effects on streamflow in the upstream regions of the Lancang-Mekong and Nu–Salween Rivers. *Journal of Hydrometeorology*, 16, 2248–2263. https://doi.org/10.1175/JHM-D-14-0238.1.

Fu, Y.H., Gao, X.J., Zhu, Y.M. and Guo, D. (2021) Climate change projection over the Tibetan Plateau based on a set of RCM simulations. *Advances in Climate Change Research*, 12, 313–321. https://doi.org/10.1016/j.accre.2021.01.004.

Gao, X.J., Shi, Y. and Giorgi, F. (2016) Comparison of convective parameterizations in RegCM4 experiments over China with CLM as the land surface model. *Atmospheric and Oceanic Science Letters*, 9, 246–254. https://doi.org/10.1080/16742834.2016.1172938.

Gao, X.J., Shi, Y., Han, Z.Y., Wang, M.L., Wu, J., Zhang, D.F., Xu, Y. and Giorgi, F. (2017) Performance of RegCM4 over major river basins in China. *Advances in Atmospheric Sciences*, 34, 441–455. https://doi.org/10.1007/s00376-016-6179-7.

Gao, X.J., Shi, Y., Zhang, D.F., Wu, J., Giorgi, F., Ji, Z.M. and Wang, Y.G. (2012) Uncertainties of monsoon precipitation projection over China: results from two high resolution RCM simulations. *Climate Research*, 52, 213–226. https://doi.org/10.3354/cr01084.

Gao, X.J., Wu, J., Shi, Y., Wu, J., Han, Z.Y., Zhang, D.F., Tong, Y., Li, R.K., Xu, Y. and Giorgi, F. (2018) Future changes in thermal comfort conditions over China based on multi-RegCM4 simulations. *Atmospheric and Oceanic Science Letters*, 11, 291–299. https://doi.org/10.1080/16742834.2018.1471578.

Gao, X.J., Xu, Y., Zhao, Z.C., Pal, J.S. and Giorgi, F. (2006) On the role of resolution and topography in the simulation of East Asia precipitation. *Theoretical and Applied Climatology*, 86, 173–185. https://doi.org/10.1007/s00704-005-0214-4.

Gao, X.J. and Zhang, D.F. (2020) Climate change of the 21st century over China from the ensemble of RegCM4 simulations. *Chinese Science Bulletin*, 65, 2516–2526 (in Chinese).

Ge, F., Peng, T., Fraedrich, K., Sielmann, F., Zhu, X., Zhi, X., Liu, X., Tang, W. and Zhao, P. (2019a) Assessment of trends and variability in surface air temperature on multiple high-resolution datasets over the Indochina Peninsula. *Theoretical and Applied Climatology*, 135, 1609–1627. https://doi.org/10.1007/s00704-018-2457-x.

Ge, F., Zhu, S., Peng, T., Zhao, Y., Sielmann, F., Fraedrich, K., Zhi, X., Liu, X., Tang, W. and Ji, L. (2019b) Risks of precipitation extremes over Southeast Asia: Does 1.5°C or 2°C global warming make a difference? *Environmental Research Letters*, 14, 044015. https://doi.org/10.1088/1748-9326/aaff7e.

Giorgi, F. (2019) Thirty years of regional climate modeling: where are we and where are we going next? *Journal of Geophysical Research: Atmospheres*, 124, 5696–5723. https://doi.org/10.1029/2018JD030094.

Giorgi, F., Coppola, E., Solmon, F., Mariotti, L., Sylla, M.B., Bi, X., Elguindi, N., Diro, G.T., Nair, V., Giuliani, G., Turuncoglu, U. U., Cozzini, S., Güttler, I., O'Brien, T.A., Tawfik, A.B., Shalaby, A., Zakey, A.S., Steiner, A.L., Stordal, F., Sloan, L.C. and Brankovic, C. (2012) RegCM4: model description and preliminary tests over multiple CORDEX domains. *Climate Research*, 52, 7–29. https://doi.org/10.3354/cr01018.

Giorgi, F. and Gao, X.J. (2018) Regional earth system modeling: review and future directions. *Atmospheric and Oceanic Science Letters*, 11, 189–197.

Giorgi, F., Hurrell, J.W., Marinucci, M.R. and Beniston, M. (1997) Elevation dependency of the surface climate change signal: a model study. *Journal of Climate*, 10, 288–296. https://doi.org/10.1175/1520-0442(1997)010<0288:EDOTSC>2.0.CO;2.

Giorgi, F., Jones, C. and Asrar, G.R. (2009) Addressing climate information needs at the regional level: the CORDEX framework. *WMO Bulletin*, 58, 175–183.

Han, Z.Y., Gao, X.J., Shi, Y., Wu, J., Wang, M. and Giorgi, F. (2015) Development of Chinese high resolution land cover for the RegCM4/CLM and its impact on regional climate simulation. *Journal of Glaciology and Geocryology*, 37, 857–866 (Chinese).

Hazeleger, W., Severijns, C., Semmler, T., Ştefănescu, S., Yang, S., Wang, X., Wyser, K., Dutra, E., Baldasano, J.M., Bintanja, R., Bougeault, P., Caballero, R., Ekman, A.M.L., Christensen, J. H., van den Hurk, B., Jimenez, P., Jones, C., Kållberg, P., Koenigk, T., McGrath, R., Miranda, P., van Noije, T., Palmer, T., Parodi, J.A., Schmith, T., Selten, F., Storelvmo, T., Sterl, A., Tapamo, H., Vancoppenolle, M., Viterbo, P. and Willén, U. (2010) EC-Earth: a seamless earth-system prediction approach in action. *Bulletin of the American Meteorological Society*, 91, 1357–1364. https://doi.org/10.1175/2010BAMS2877.1.

Hijioka, Y., Lin, E., Pereira, J.J., Corlett, R.T., Cui, X., Insarov, G.E., Lasco, R.D., Lindgren, E. and Surjan, A. (2014) Asia. In: Barros, V.R., Field, C.B., Dokken, D.J., Mastrandrea, M.D., Mach, K.J., Bilir, T.E., Chatterjee, M., Ebi, K.L., Estrada, Y.O., Genova, R.C., Girma, B., Kissel, E.S., Levy, A.N., MacCracken, S., Mastrandrea, P.R. and White, L.L. (Eds.) *Climate Change 2014: Impacts, Adaptation, and Vulnerability. Part B: Regional Aspects. Contribution of Working Group II to the Fifth Assessment Report of the Intergovernmental Panel on Climate Change*. Cambridge and New York, NY: Cambridge University Press, pp. 1327–1370.

Huang, Y., Wang, F.Y., Li, Y. and Cai, T.J. (2014) Multi-model ensemble simulation and projection in the climate change in the Mekong River basin. Part I: temperature. *Environmental Monitoring and Assessment*, 186, 7513–7523. https://doi.org/10.1007/s10661-014-3944-x.

Iqbal, Z., Shahid, S., Ahmed, K., Ismail, T., Ziarh, G.F., Chung, E.-S. and Wang, X. (2021) Evaluation of CMIP6 GCM rainfall in mainland Southeast Asia. *Atmospheric Research*, 254, 105525. https://doi.org/10.1016/j.atmosres.2021.105525.

Irannezhad, M., Liu, J. and Chen, D. (2020) Influential climate teleconnections for spatiotemporal precipitation variability in the Lancang-Mekong River basin from 1952 to 2015. *Journal of Geophysical Research: Atmospheres*, 125(21), e2020JD033331. https://doi.org/10.1029/2020JD033331.

Iversen, T., Bentsen, M., Bethke, I., Debernard, J.B., Kirkevåg, A., Seland, Ø., Drange, H., Kristjansson, J.E., Medhaug, I., Sand, M. and Seierstad, I.A. (2013) The Norwegian earth system model, NorESM1-M-part 2: climate response and scenario projections. *Geoscientific Model Development*, 6, 389–415. https://doi.org/10.5194/gmd-6-389-2013.

Jiang, D.B. and Fu, Y.H. (2012) Climate change over China with a 2°C global warming. *Chinese Journal of Atmospheric Sciences*, 36, 234–246 (in Chinese).

Jiang, D.B., Tian, Z.P. and Lang, X.M. (2016) Reliability of climate models for China through the IPCC third to fifth assessment reports. *International Journal of Climatology*, 36, 1114–1133. https://doi.org/10.1002/joc.4406.

Jungclaus, J.H., Fischer, N., Haak, H., Lohmann, K., Marotzke, J., Matei, D., Mikolajewicz, U., Notz, D. and von Storch, J.S. (2013) Characteristics of the ocean simulations in the Max Planck Institute Ocean Model (MPIOM) the ocean component of the MPI-Earth system model. *Journal of Advances in Modeling Earth Systems*, 5, 422–446. https://doi.org/10.1002/jame.20023.

Katzfey, J., Nguyen, K., McGregor, J., Hoffmann, P., Ramasamy, S., Nguyen, H.V., Khiem, M.V., Nguyen, T.V., Truong, K.B., Vu, T. V., Nguyen, H.T., Thuc, T., Phong, D.H., Nguyen, B.T., Phan-van, T., Nguyen-Quang, T., Ngo-Duc, T. and Trinh-Tuan, L. (2016) High-resolution simulations for Vietnam—methodology and evaluation of current climate. *Asia-Pacific Journal of Atmospheric Sciences*, 52, 91–106. https://doi.org/10.1007/s13143-016-0011-2.

Lee, J.Y., Marotzke, J., Bala, G., Cao, L., Corti, S., Dunne, J.P., Engelbrecht, F., Fischer, E., Fyfe, J.C., Jones, C., Maycock, A., Mutemi, J., Ndiaye, O., Panickal, S. and Zhou, T. (2021) Future global climate: scenario based projections and near-term information. In: Masson-Delmotte, V., Zhai, P., Pirani, A., Connors, S.L., Péan, C., Berger, S., Caud, N., Chen, Y., Goldfarb, L., Gomis, M. I., Huang, M., Leitzell, K., Lonnoy, E., Matthews, J.B.R., Maycock, T.K., Waterfield, T., Yelekçi, O., Yu, R. and Zhou, B. (Eds.) *Climate Change 2021: The Physical Science Basis. Contribution of Working Group I to the Sixth Assessment Report of the Intergovernmental Panel on Climate Change*. Cambridge and New York, NY: Cambridge University Press. (in press).

Liu, J.G., Chen, D.L., Mao, G.Q., Irannezhad, M. and Pokhrel, Y. (2021) Past and future changes in climate and water resources in the Lancang-Mekong River basin: current understanding and future research directions. *Engineering*, 13, 144–152.

Manton, M.J., Della-Marta, P.M., Haylock, M.R., Hennessy, K.J., Nicholls, N., Chambers, L.E., Collins, D.A., Daw, G., Finet, A., Gunawan, D., Inape, K., Isobe, H., Kestin, T.S., Lefale, P., Leyu, C.H., Lwin, T., Maitrepierre, L., Ouprasitwong, N., Page, C.M., Pahalad, J., Plummer, N., Salinger, M.J., Suppiah, R., Tran, V.L., Trewin, B., Tibig, I. and Yee, D. (2001) Trends in extreme daily rainfall and temperature in Southeast Asia and the South Pacific: 1961–1998. *International Journal of Climatology*, 21, 269–284. https://doi.org/10.1002/joc.610.

Mekong River Commission (MRC). (2005) *Overview of the hydrology of the Mekong basin*. Vientiane, Lao PDR: Mekong River Commission. Available at: http://www.mekonginfo.org/assets/midocs/0001968-inland-waters-overview-of-the-hydrology-of-the-mekong-basin.pdf.

Mekong River Commission (MRC). (2010) *State of the basin report 2010*. Vientiane, Lao PDR: Mekong River Commission. Available at: https://www.mrcmekong.org/assets/Publications/basin-reports/MRC-SOB-report-2010full-report.pdf.

Ngo-Duc, T., Tangang, F.T., Santisirisomboon, J., Cruz, F., Trinh-Tuan, L., Nguyen-Xuan, T., Phan-van, T., Juneng, L., Narisma, G., Singhruck, P., Gunawan, D. and Aldrian, E. (2017) Performance evaluation of RegCM4 in simulating extreme rainfall and temperature indices over the CORDEX-Southeast Asia region. *International Journal of Climatology*, 37, 1634–1647. https://doi.org/10.1002/joc.4803.

Nguyen-Ngoc-Bich, P., Phan-Van, T., Ngo-Duc, T., Vu-Minh, T., Trinh-Tuan, L., Tangang, F.T., Liew, J., Cruz, F., Santisirisomboon, J., Narisma, G. and Aldrian, E. (2021) Projected evolution of drought characteristics in Vietnam based on CORDEX-SEA downscaled CMIP5 data. *International Journal of Climatology*, 41, 5733–5751. https://doi.org/10.1002/joc.7150.

Nguyen-Thuy, H., Ngo-Duc, T., Trinh-Tuan, L., Tangang, F., Cruz, F., Phan-Van, T., Juneng, L., Narisma, G. and Santisirisomboon, J. (2020) Time of emergence of climate signals over Vietnam detected from the CORDEX-SEA experiments. *International Journal of Climatology*, 41, 1599–1618. https://doi.org/10.1002/joc.6897.

Olson, R., Evans, J.P., Di Luca, A. and Argüeso, D. (2016) The NARCliM project: model agreement and significance of climate projections. *Climate Research*, 69, 209–227. https://doi.org/10.3354/cr01403.

Overland, I., Azlan, L., Charadine, P., Chongokittavorn, K., Esksuriya, C., Estrada, E., Husain, S.A., Jaabi, A., Lemphers, N., Mohdyatid, M., Nguyen, H., Parcon, R., Pek, S., Perkasa, V., Selamat, F., Siborliboun, C., Sothirak, P., Sunchindah, A., Thein, K., Tin,D., Vakulchuk, R., Wijaya, A. and Zainul, H. (2017) *Impact of Climate Change on ASEAN International Affairs: Risk and Opportunity Multiplier*. Norwegian Institute of International Affairs and Myanmar Institute of International and Strategic Studies. Available at: https://www.researchgate.net/publication/320622312_Impact_of_Climate_Change_on_ASEAN_International_Affairs_Risk_and_Opportunity_Multiplier.

Rotstayn, L.D., Collier, M.A., Dix, M.R., Feng, Y., Gordon, H.B., O'Farrell, S.P., Smith, I.N. and Syktus, J. (2010) Improved simulation of Australian climate and ENSO-related rainfall variability in a global climate model with an interactive aerosol treatment. *International Journal of Climatology*, 30, 1067–1088. https://doi.org/10.1002/joc.1952.

Ruan, Y., Liu, Z., Wang, R. and Yao, Z. (2019) Assessing the performance of CMIP5 GCMs for projection of future temperature change over the lower Mekong basin. *Atmosphere*, 10, 93. https://doi.org/10.3390/atmos10020093.

Sørland, S.L., Schar, C., Luthi, D. and Kjellstrom, K. (2018) Bias patterns and climate change signals in GCM-RCM model chains. *Environmental Research Letters*, 13, 074017. https://doi.org/10.1088/1748-9326/aacc77.

Stevens, B., Giorgetta, M., Esch, M., Mauritsen, T., Crueger, T., Rast, S., Salzmann, M., Schmidt, H., Bader, J., Block, K., Brokopf, R., Fast, I., Kinne, S., Kornblueh, L., Lohmann, U., Pincus, R., Reichler, T. and Roeckner, E. (2013) Atmospheric component of the MPI-M Earth System Model: ECHAM6. *Journal of Advances in Modeling Earth Systems*, 5, 146–172. https://doi.org/10.1002/jame.20015.

Sun, C., Xiao, Z., Sun, J. and Yu, E. (2020) Projection of temperature change and extreme temperature events in the Lancang-Mekong River basin. *Atmospheric and Oceanic Science Letters*, 13, 16–25. https://doi.org/10.1080/16742834.2020.1696143.

Supari, Tangang, F., Juneng, L. and Aldrian, E. (2017) Observed changes in extreme temperature and precipitation over Indonesia. *International Journal of Climatology*, 37, 1979–1997. https://doi.org/10.1002/joc.4829.

Supari, Tangang, F., Juneng, L., Cruz, F., Chung, J., Ngai, S., Salimun, E., Mohd, M., Santisirisomboon, J., Singhruck, P., Phan-Van, T., Ngo-Duc, T., Narisma, G., Aldrian, E., Gunawan, D. and Sopaheluwakan, A. (2020) Multi-model projections of precipitation extremes in Southeast Asia based on CORDEX-Southeast Asia simulations. *Environmental Research*, 184, 109350. https://doi.org/10.1016/j.envres.2020.109350.

Supharatid, S., Nafung, J. and Aribarg, T. (2022) Projected changes in temperature and precipitation over mainland Southeast Asia by CMIP6 models. *Journal of Water and Climate Change*, 13, 337–356. https://doi.org/10.2166/wcc.2021.015.

Tang, J.P., Li, Q., Wang, S.Y., Lee, D.K., Hui, P.H., Niu, X.R., Gutowski, W.J., Dairaku, K., McGregor, J., Katzfey, J., Gao, X., Wu, J., Hong, S., Wang, Y. and Sasaki, H. (2016) Building Asian climate change scenario by multi-regional climate models ensemble. Part I: surface air temperature. *International Journal of Climatology*, 36, 4241–4252. https://doi.org/10.1002/joc.4628.

Tangang, F., Juneng, L. and Ahmad, S. (2007) Trend and interannual variability of temperature in Malaysia: 1961–2002. *Theoretical and Applied Climatology*, 89, 127–141. https://doi.org/10.1007/s00704-006-0263-3.

Tangang, F., Supari, S., Chung, J.X., Cruz, F., Salimun, E., Ngai, S. T., Juneng, L., Santisirisomboon, J., Santisirisomboon, J., Ngo-Duc, T., Phan-van, T., Narisma, G., Singhruck, P., Gunawan, D., Aldrian, E., Sopaheluwakan, A., Nikulin, G., Yang, H., Remedio, A.R.C., Sein, D. and Hein-Griggs, D. (2018) Future changes in annual precipitation extremes over Southeast Asia under global warming of 2°C. *APN Science Bulletin*, 8, 3-8. https://doi.org/10.30852/sb.2018.436.

Tangang, F., Chung, J., Juneng, L., Supari, Salimun, E., Ngai, S., Jamaluddin, A., Mohd, M., Cruz, F., Narisma, G., Santisirisomboon, J., Ngo-Duc, T., Tan, P., Singhruck, P., Gunawan, D., Aldrian, E., Sopaheluwakan, A., Grigory, N., Remedio, A., Sein, D., Hein-Griggs, D., McGregor, J., Yang, H., Sasaki, H. and Kumar, P. (2020) Projected future changes in rainfall in Southeast Asia based on CORDEX–SEA multi-model simulations. *Climate Dynamics*, 55, 1247–1267. https://doi.org/10.1007/s00382-020-05322-2.

Taylor, K.E. (2001) Summarizing multiple aspects of model performance in a single diagram. *Journal of Geophysical Research*, 106, 7183–7192. https://doi.org/10.1029/2000JD900719.

Taylor, K.E., Stouffer, R.J. and Meehl, G.A. (2012) An overview of CMIP5 and the experiment design. *Bulletin of the American Meteorological Society*, 93, 485–498. https://doi.org/10.1175/BAMS-D-11-00094.1.

Thirumalai, K., DiNezio, P., Okumura, Y. and Deser, C. (2017) Extreme temperatures in Southeast Asia caused by El Niño and worsened by global warming. *Nature Communications*, 8, 15531. https://doi.org/10.1038/ncomms15531.

Tong, Y., Gao, X.J., Han, Z.Y., Xu, Y.Q., Xu, Y. and Giorgi, F. (2020) Bias correction of temperature and precipitation over China from a series of RCM simulations using QM and QDM methods. *Climate Dynamics*, 57, 1425–1443. https://doi.org/10.1007/s00382-020-05447-4.

Wu, J. and Gao, X.J. (2013) A gridded daily observation dataset over China region and comparison with the other datasets. *Chinese Journal of Geophysics*, 56, 1102–1111 (in Chinese).

Wu, J. and Gao, X.J. (2020) Present day bias and future change signal of temperature over China in a series of multi-GCM driven RCM simulations. *Climate Dynamics*, 54, 1113–1130. https://doi.org/10.1007/s00382-019-05047-x.

Wu, J., Gao, X.J., Shi, Y. and Giorgi, F. (2021) Projection of the future changes in tropical cyclones activity over the western

North Pacific based on multi-RegCM4 simulations. *Advances in Atmospheric Sciences*, 39, 284–303. https://doi.org/10.1007/s00376-021-0286-9.

Yatagai, A., Kaminguchi, K., Arakawa, O., Hamada, A. and Kitoh, A. (2012) APHRODITE: constructing a long-term daily gridded precipitation dataset for Asia based on a dense network of rain gauges. *Bulletin of the American Meteorological Society*, 93, 1401–1415. https://doi.org/10.1175/BAMS-D-11-00122.1.

How to cite this article: Fu, Y., Gao, X., Xu, Y., & Giorgi, F. (2022). Climate change projection over Mainland Southeast Asia and the Lancang-Mekong River basin based on a set of RegCM4 simulations. *International Journal of Climatology*, 1–19. https://doi.org/10.1002/joc.7811